First-principles simulations of native point defects and ionic diffusion in high-pressure polymorphs of silica

Ashok K. Verma* and Bijaya B. Karki
Department of Computer Science and Department of Geology and Geophysics, Louisiana State University, Baton Rouge, Louisiana 70803, USA
(Received 23 March 2009; revised manuscript received 9 May 2009; published 24 June 2009)

Several native point defects including vacancies, interstitials, and their complexes were studied in high-pressure polymorphs of silica (stishovite, $CaCl_2$, α-PbO_2, and pyrite types) up to 200 GPa within density-functional theory. The formation enthalpies of the individual defects strongly depend on atomic chemical potentials and the Fermi level. Their values were shown to increase by a factor of 2 over the entire pressure range studied with large differences in some cases between different phases. The Schottky defects are energetically most favorable at zero pressure whereas O-Frenkel pairs become systematically more favorable at pressures higher than 20 GPa. The activation enthalpies of ionic migrations obtained by the nudged-elastic-band method suggest that the interstitial mechanisms are favored over the vacancy hoping mechanisms. The geometric and electronic structures of defects and migrating ions vary largely among different types of defects. In particular, the O defects introduce localized electronic states. These structures remain qualitatively unchanged with compression showing similar trends among different polymorphs.

DOI: 10.1103/PhysRevB.79.214115 PACS number(s): 83.80.Nb, 61.72.J−, 71.15.Mb

I. INTRODUCTION

Silica is one of the most widely studied materials due to its great technological and geological importance. Theoretical and experimental studies have shown that silica undergoes a series of pressure-induced structural transformations thereby adopting six polymorphs, namely, α quartz, coesite, stishovite, $CaCl_2$ type, α-PbO_2 type, and pyrite type over the pressure regime of a couple of hundreds of gigapascals. These transformations are expected or shown to influence a wide range of physical properties of silica including widely studied structure, thermodynamics, and elasticity [e.g., Refs. 1–3]. However, our knowledge about point defects in silica is still limited. Point defects related to silicon and oxygen vacancies and interstitials in α quartz have been previously studied extensively.[4–10] However, such studies are still lacking for the high-pressure phases. In particular, some fundamental questions are yet to be answered: how do the properties of point defects vary with pressure in the case of silica? What are the effects of the phase transformations on energetics, geometric, and electronic structures associated with point defects and ion migration? The answers to these questions are critical to our understanding of rheological properties of solid materials under compression. Point defects are responsible for mediating self-diffusion. Minerals in mantle rocks are known to deform by a diffusional creep mechanism[11,12] and the creep rate is controlled by the slowest moving ionic species.[13] Ionic diffusion also controls electrical conductivity in minerals.[14] Information about dominant defects and their migrations in silica, being an important component of Earth's crust and mantle, is expected to be useful in modeling of rheology and conductivity of Earth's interior.[12,14]

An accurate computational study of defects demands first-principles simulations with relatively large supercells, which have become feasible in recent years (e.g., Refs. 15–18). These simulations make no assumptions to the nature of bonding or the shape of the charge density and are thus in principles equally applicable in the study of a wide variety of properties including defects, which are likely to be determined by local bonding. In this paper, we report first-principles investigations of various point defects and their migration in silica considering four polymorphs, stishovite (0 and 50 GPa), $CaCl_2$-type (80 GPa), α-PbO_2-type (150 GPa), and finally pyrite-type (200 GPa). Individual defects (vacancies and interstitials) in the neutral and charge states were calculated to study their dependence on atomic and electronic chemical potentials. We also study charge-balanced stoichiometry-preserving defects (Schottky triplets and Frenkel pairs), which have well-defined energies. For instance, the Schottky defects require simulations of ionic vacancies with charge states of 4− and 2+ on cationic (Si) and anionic (O) sites, respectively. We present and discuss the results for the enthalpies and volumes of defect formation and ionic migration, and also analyze the defect-induced atomic and electronic structures. By studying four polymorphs, we expect to provide important insight into how the defect properties vary with pressure and across the structural transformations in silica.

II. METHODOLOGY

Our calculations are based on density-functional theory within the local-density approximation (LDA) as implemented in QUANTUM-ESPRESSO code.[19] The supercells consist of 72 atoms for stishovite and $CaCl_2$-type, and 96 atoms for α-PbO_2- and pyrite-type phases. The pseudopotentials for Si and O, and the plane-wave cutoff of 70 Ry are the same as those were used in our previous studies.[17] The Brillouin zone was sampled with $2\times2\times2$ Monkhorst-Pack mesh.[20] The results were well converged with respect to the system size, plane-wave cutoff, $\boldsymbol{k}$-point sampling, and the choice of the exchange-correlation function. For instance, the Schottky defect formation enthalpies differ by less than 0.2 eV between different supercell sizes used. Similarly, the differences be-

 ©2009 The American Physical Society

tween LDA and GGA (Ref. 21) are within 0.5 eV even for α quartz.[9]

In the past, first-principles calculations of defects were mostly performed at the ambient pressure. How these calculations should be performed at a finite pressure is not well documented in the literature. So we feel that it is useful to describe the method in some details. We start with the case of a single defect in an elemental system assuming that the defect is a vacancy in the neutral state. The formation enthalpy of this vacancy defect at a pressure P is defined as[22]

$$H_f(P) = E_f(P) + P\Omega_f(P), \quad (1)$$

where E_f and Ω_f are the defect formation energy and volume, respectively. We can express these quantities in terms of the system internal energy and volume,

$$E_f(P) = E(N-1,P) - \frac{N-1}{N}E(N,P) = E(N-1,P) - E(N,P) + \frac{E(N,P)}{N}, \quad (2)$$

$$\Omega_f(P) = V(N-1,P) - \frac{N-1}{N}V(N,P) = V(N-1,P) - V(N,P) + \frac{V(N,P)}{N}. \quad (3)$$

Here, $E(N,P)$ and $V(N,P)$ are the internal energy and volume, respectively, of a perfect crystal containing N lattice sites at pressure P whereas $E(N-1,P)$ and $V(N-1,P)$ are the corresponding quantities of a defective system containing one vacancy site (i.e., one atom missing) at the same pressure. The expression for H_f can be rewritten as

$$H_f(P) = E(N-1,P) - E(N,P) + P\Delta V + \mu(P), \quad (4)$$

where

$$\Delta V = V(N-1,P) - V(N,P) \quad (5)$$

is the volume difference between the defective and prefect supercells, and

$$\mu(P) = \frac{E(N,P) + PV(N,P)}{N} = \frac{H(N,P)}{N} \quad (6)$$

is the atomic chemical potential that represents the enthalpy of the reservoir with which the atoms are exchanged when assembling the crystal in question. Thus, the value of μ which simply defines the reference state of the atom is a well-defined quantity, i.e., the enthalpy of the crystal per atom.

In the constant-volume approach used in this work, $\Delta V = 0$ so that the defect formation enthalpy is given by

$$H_f(P) = E(N-1,V) - E(N,V) + \mu(P), \quad (7)$$

here μ still represents the enthalpy of the reservoir at pressure P corresponding to the perfect system volume V at which the defect calculation is performed. Thus, we need to calculate the relaxed total energy, $E(N,V)$, of perfect supercell and that, $E(N-1,V)$, of the defective supercell with one atom missing. In the constant-volume approach [e.g., Refs. 15, 17, and 23], the perfect crystal is first fully optimized with respect to its internal and cell parameters as a function of pressure. Defect calculations are then performed by keeping the volume fixed, i.e., the cell parameters of the defect-containing supercell are not allowed to relax but ionic positions are fully relaxed. Due to the finite-size supercell used, the defect concentration of the simulated system turns out to be relatively high, i.e., the system corresponds to an ordered array of defects at a high concentration. For example, one vacancy defect in a 72 atom system corresponds to a concentration of ~1.4%. However, our calculations are meant for a single defect in an infinite system for which the lattice constants should correspond to those that are optimized for the bulk of unit cell. The constant-volume method used here avoids any spurious elastic interactions with defects in the neighboring supercells, which otherwise result in a large volume change. A review by Nieminen[24] has discussed various issues with the supercell method for defect calculations. On the other hand, a constant pressure approach would in fact correspond to finding the lattice parameters (and volume) of the system containing an ordered array of defects at a high concentration.[9,22] It can be shown that the constant pressure method with appropriate $P\Delta V$ term reproduces the results from the constant-volume simulations.[17]

Now, we define the formation enthalpy of a defect D of a charge state q in a compound system (e.g., Refs. 24–26) as

$$H_f(D^q,P) = E_{tot}(D^q) - E_{tot}^{perf} + n_X\mu_X(P) + q\mu_e - \Delta E_{DD}(q,P). \quad (8)$$

Here, the first and second terms are, respectively, $E(N-1,V)$ and $E(N,V)$. $\mu_X(P)$ is the atomic chemical potential (i.e., the reference state) of the removed/added atom (μ_{Si} for Si atom or μ_{O} for O atom in the case of silica) at pressure P. The value of n_X is 1 for a vacancy defect (i.e., an atom is removed from the crystal) and −1 for an interstitial defect (i.e., an atom is added to the crystal). Unlike a monoatomic (i.e., elemental) system discussed earlier, the individual atomic chemical potentials for a compound are not known exactly. Only the chemical potential of the SiO_2 unit is well defined, which is simply the enthalpy of the bulk compound per formula unit, i.e., $\mu_{\mathrm{SiO_2}} = \mu_{\mathrm{Si}} + 2\mu_{\mathrm{O}}$. The single atom energies depend on the interactions of crystal and its environment. For instance, in the O-rich condition, O atoms may be removed from the crystal and added to the reservoir. The energy of O atoms in the reservoir is constant and in thermal equilibrium with the crystal. The O energy now determines the Si energy since these two energies also determine the total energy of the bulk silica. Thus, the individual chemical potentials (μ_{Si} and μ_{O}) vary between the Si-rich and O-rich limits, which are determined by the chemical potentials of stable bulk Si phase and bulk (or molecular at zero pressure) O phase, denoted as $\mu_{\mathrm{Si}}^{\mathrm{B}}$ and $\mu_{\mathrm{O}}^{\mathrm{B}}$. If $\Delta H = (\mu_{\mathrm{Si}}^{\mathrm{B}} + 2\mu_{\mathrm{O}}^{\mathrm{B}}) - \mu_{\mathrm{SiO_2}}$ is the heat of formation then the two types of atomic potentials are related as, $\mu_{\mathrm{Si}} = \mu_{\mathrm{Si}}^{\mathrm{B}} - \lambda\Delta H$ and $\mu_{\mathrm{O}} = \mu_{\mathrm{O}}^{\mathrm{B}} - (1-\lambda)\Delta H/2$, where λ varies between 0 and 1. Thus, the Si-rich limit ($\lambda = 0$) corresponds to the upper limit of $\mu_{\mathrm{Si}} = \mu_{\mathrm{Si}}^{\mathrm{B}}$ and also to the lower limit of $\mu_{\mathrm{O}} = (\mu_{\mathrm{SiO_2}} - \mu_{\mathrm{Si}}^{\mathrm{B}})/2$. Similarly, the O-rich limit

($\lambda=1$) corresponds to the upper limit of $\mu_{\mathrm{O}}=\mu_{\mathrm{O}}^{\mathrm{B}}$ and also to the lower limit of $\mu_{\mathrm{Si}}=\mu_{\mathrm{SiO}_2}-2\mu_{\mathrm{O}}^{\mathrm{B}}$. The enthalpies of the respective Si, O, and silica phases as a function of pressure were used to determine $\mu_{\mathrm{Si}}^{\mathrm{B}}$, $\mu_{\mathrm{O}}^{\mathrm{B}}$, and μ_{SiO_2}, respectively, at each pressure.

The defect formation enthalpy for a charged defect also depends on the Fermi level, which was used here as the chemical potential (μ_e) of electrons. If $q>0(q<0)$, $|q|$ electrons are transferred from (to) an electron reservoir. The Fermi level is measured relative to the valence-band maximum (VBM) for the bulk material. The energy of the top of the valence band in a defective cell is different from that in a perfect supercell because of the finite-size supercell used under periodic boundary conditions. Therefore, it is necessary to line up the VBM between the perfect and defective supercells. We overcome this problem by including the defect-defect correction term given by[27,28] $\Delta E_{DD}(q,P)=-\alpha q^2/2\varepsilon L=-\alpha^* q^2/\varepsilon$, where α is the appropriately defined Madelung constant for the supercell of the length L. We use the direct Ewald sum method to compute the value of α^* as a function of P as in previous studies.[15,17] The static values of dielectric constant (ε) taken from first-principles lattice dynamics calculations of stishovite and CaCl_2 phase[29] were used and extrapolated for other phases.

As discussed above, the formation enthalpy of a charged defect being dependent on the choice of the external reservoir and the Fermi level needs to be calculated as a function of λ and μ_e. There are situations that conserve the relative number of charged defects and hence give well-defined energetics independent of the values of λ and μ_e. They are the charge-balanced stoichiometry-preserving defects of Schottky and Frenkel types, which can be unambiguously defined since the Si and O atoms are not removed to infinity from the solid. In the case of Schottky defects, the atoms removed from crystal sites are used to create a formula unit of the same phase on the surface whereas in the case of Frenkel pairs, those atoms are placed at interstitial sites. Both defect types are often considered among the most common point defects in solid materials. We use the above defined formation enthalpies for Si and O vacancies [Eq. (8)] to calculate the Schottky triplet formation enthalpy (per defect) as follows:

$$H_f^S(P)=\frac{1}{3}[H_f(V_{\mathrm{Si}}^{4-},P)+2H_f(V_{\mathrm{O}}^{2+},P)], \tag{9}$$

which can be rewritten as

$$3H_f^S(P)=[E_{tot}(V_{\mathrm{Si}}^{4-})-E_{tot}^{perf}]+2[E_{tot}(V_{\mathrm{O}}^{2+})-E_{tot}^{perf}]+\mu_{\mathrm{SiO}_2}(P) -[\Delta E_{DD}(4-,P)+2\Delta E_{DD}(2+,P)]. \tag{10}$$

Note that the second representation [Eq. (10)] contains the enthalpy (chemical potential) of one formula (SiO_2) unit, which can be determined from the silica bulk calculation, and only the charge dependent term is the defect-defect correction. Similarly, for a Frenkel pair, the formation enthalpy per defect is

$$H_f^F(D^q,P)=\frac{1}{2}[H_f(V_X^q,P)+H_f(X_I^{q-},P)], \tag{11}$$

which can be written as

$$2H_f^F(D^q,P)=[E_{tot}(V_X^q)-E_{tot}^{perf}]+[E_{tot}(X_I^{q-})-E_{tot}^{perf}] -\Delta E_{DD}(q,P)-\Delta E_{DD}(q-,P). \tag{12}$$

The Frenkel pair formation enthalpy using Eq. (12) can be also determined without the knowledge of the individual vacancy and interstitial formation enthalpies.

III. RESULTS AND DISCUSSION

A. Formation Enthalpies

We calculate the formation enthalpies of several defects (vacancies and interstitials in different charge states) using Eq. (8) as a function of the Fermi level and λ for four high-pressure phases of silica (Fig. 1). As discussed below, the defect formation enthalpies strongly depend on the electronic chemical potential (μ_e—the Fermi level) and the atomic chemical potentials (μ_{Si} and μ_{O}). We first discuss the results for stishovite at 0 GPa (Fig. 1, top row) and then discuss how they vary with pressure through structural phase transformations.

For each defect type (vacancy or interstitial), the energetic favorability depends on the Fermi level. At zero pressure for stishovite, the calculated band gap is 5.76 eV and the Fermi level can change its position within the band gap. The energetically most favorable charge state varies with μ_e, and the Fermi level where the formation enthalpy for a charge state equals to that for another charge state determines the defect transition energy. Note that μ_e is measured from the VBM. For Si vacancies, the transition from 2− to 4− occurs at 1.1 eV from the VBM [dashed lines in Fig. 1(a), top] whereas for O vacancies, two transitions occur; first from 2+ to 0 at 1.2 eV and then to 2− at 5.3 eV (dashed lines in Fig. 1(b), top). The second transition energy is very close to the conduction-band minimum (CBM). The Si-interstitial defect shows three successive transitions; first 4+ to 2+ at 2.9 eV, then to 0 at 4.1 eV, and finally to 2− at 5.5 eV [solid lines Fig. 1(a), top]. On the other hand, the O interstitial defect is energetically favorable in the 1+ state in a short energy range up to 0.2 eV at which the neutral state (0) becomes the most favorable and then finally beyond 3 eV the 2− state becomes the most favorable [solid lines in Fig. 1(b), top]. The predicted defect transition sequences and energies remain the same with respect to the atomic chemical potentials; the lines showing the defects of each type are shifted up or down relative to each other between left (Si-rich limit) and right (O-rich limit) in Fig. 1.

In the previous paragraph, we have identified the energetically most favorable charge states for each defect type (Si-vacancies, Si-interstitials, O-vacancies, and O-interstitials). When defects of all types are considered together, the energetic favorability is also dependent on the values of atomic chemical potentials (note that μ_{Si} and μ_{O} are interdependent through λ). This is because the formation enthalpies of defects of different types are affected by different amounts de-

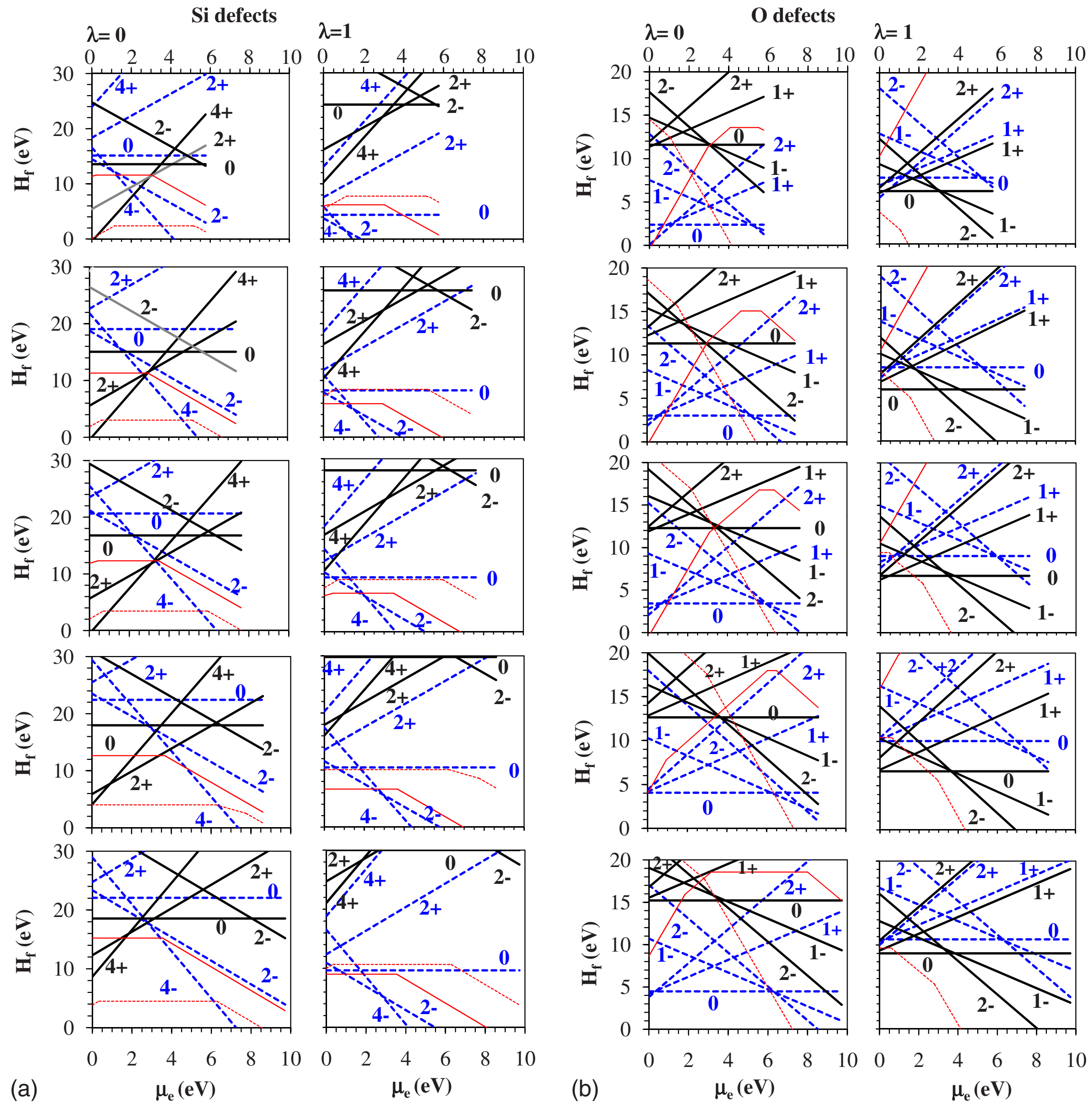

FIG. 1. (Color online) Calculated formation enthalpies (H_f) of (a) Si and (b) O defects in silica as a function of electron chemical potential. Vacancies (dashed lines) and interstitials (solid lines) are shown in the Si-rich (λ=0) and O-rich (λ=1) limits. The numbers alongside the lines denote the charges associated with the defects. From the top to the bottom are stishovite (0 and 50 GPa), $CaCl_2$ phase (80 GPa), α-PbO_2 phase (150 GPa), and pyrite phase (200 GPa). The thin (red) lines represent the lowest energy vacancy (dashed lines) and interstitial (solid lines) defects for O in (a) and Si in (b).

pending on the value of λ. Going from λ=0 to λ=1, the Si-vacancy formation enthalpies are shifted down by 10.8 eV whereas the Si-interstitial formation enthalpies are shifted up by the same amount. Over the same range of λ, the O-vacancy and interstitial formation enthalpies show an opposite trend, i.e., their respective values are shifted upward and downward by a half amount (5.4 eV). Among all the defects studied, for λ=0 (i.e., the Si-rich condition), the defects having the lowest formation enthalpies are Si_I^{4+} (for μ_e=0 to 0.2 eV), V_O^{2+} (for μ_e=0.2 to 1.2 eV), V_O^0 (for μ_e =1.2 to 3.6 eV) and V_{Si}^{4-} (for μ_e above 3.6 eV) for the μ_e values lying within the band gap. Note that the dominant defects of other species are shown in Fig. 1 by thin lines. When λ=1 (i.e., the O-rich condition), Si-vacancies become most favored with V_{Si}^{2-} (for μ_e=0.0 to 1.2 eV) and V_{Si}^{4-} (for μ_e above 1.1 eV). Thus, it is the Si and O vacancies that are likely the most dominant individual defects in stishovite at the ambient pressure.

Our results show in most cases monotonic trends for the pressure variations in individual defect formation enthalpies with their values increasing as pressure increases up to 150 GPa (Fig. 1). This pressure range covers three phases, stishovite (0 and 50 GPa), $CaCl_2$ type (80 GPa), and α-PbO_2 type (150 GPa). Moreover, the effects of pressure are more or less uniform among the defects of a given type. The Si-vacancies and interstitials show much larger pressure variations (by a factor of 2) than the O vacancies and interstitials do. The formation enthalpies of some defects (in particular, Si and O vacancies) abruptly drop across the α-PbO_2 to pyrite phase transition. The predicted energetic favorability among defects of a given type changes somewhat with pressure. For instance, unlike a single Si-vacancy transition (from 2− to

TABLE I. Information about supercells used. The experimental data at the ambient conditions are from Ref. 35. Also shown are the calculated band gaps, and the Fermi-level positions determined by the charge neutrality condition at 2000 K.

P (GPa)	Phase	Cell parameters a, b, c (Å)	N	Band gap (eV)	μ_e (eV) Si-rich	μ_e (eV) O-rich
0	Stishovite	8.328, 8.328, 8.019	72	5.76	2.89	0.88
	Expt.	8.354, 8.354, 7.998				
50	Stishovite	7.964, 7.964, 7.774	72	7.38	3.57	1.96
80	$CaCl_2$	7.623, 7.976, 7.617	72	7.61	3.80	2.62
150	α-PbO_2	7.338, 9.225, 8.239	96	8.60	4.29	3.24
200	Pyrite	8.001, 8.001, 8.001	96	9.72	4.75	3.14

4−) predicted for stishovite (at 0 and 50 GPa), two transitions were found for $CaCl_2$ (80 GPa), α-PbO_2 (150 GPa) and pyrite (200 GPa) phases. The neutral Si vacancy is favored over the 2− and 4− states in the vicinity of the VBM (for $\mu_e < \sim 0.5$ eV) for these phases. With increasing pressure, the 2− to 4− transition systematically shifts away from the VBM (occurring at 1.5, 2.2, 2.9, and 2.8 eV, respectively, at 50, 80, 150 and 200 GPa, compared to 1.1 eV at 0 GPa). Also, the overall energetic favorability is sensitive to pressure. In the Si-rich condition, as pressure increases, only V_{O}^{0} and V_{Si}^{4-} among four favorable defects at 0 GPa continue to have the lowest energy depending on the value of the Fermi level. On the other hand in the O-rich condition, at high pressures the interstitial neutral O has the lowest energy in the vicinity of the VBM whereas Si vacancies have the lowest energies for μ_e values away from the VBM. Note that the range of μ_e over which a given defect has the lowest energy varies with pressure.

The negative formation enthalpies of the charged defects are not feasible since the corresponding extreme values of atomic and electron chemical potentials cannot be obtained simultaneously by the charge neutrality requirements. The charge neutrality equation represents a balance between the concentrations of all charged defects through their influence on the Fermi level (i.e., involving electron and hole concentrations),

$$\sum_D q_D c_D - n + p = 0. \tag{13}$$

Here, $c_D = N \exp[-H_f^D / k_B T]$ represents the concentration of a defect D (vacancy or interstitial) carrying the charge q_D, which is proportional to the number (N) of sublattice sites per unit volume. The electron concentration n and hole concentration p are approximated from the calculated density of states using the Fermi-Dirac distributions. The Fermi level is considered as a variable and its value at given temperature (T) and external condition (λ) is determined by the charged neutrality [defined by Eq. (13)] between concentrations of charged defects, electrons, and holes. Note that we have neglected the vibrational entropy contributions and also assumed that formation enthalpies are independent of temperature. The calculated Fermi energies (Table I) and three types of concentrations (Fig. 2) for all silica polymorphs were calculated at 2000 K. The choice of such a high temperature represents the geophysically relevant temperatures of the

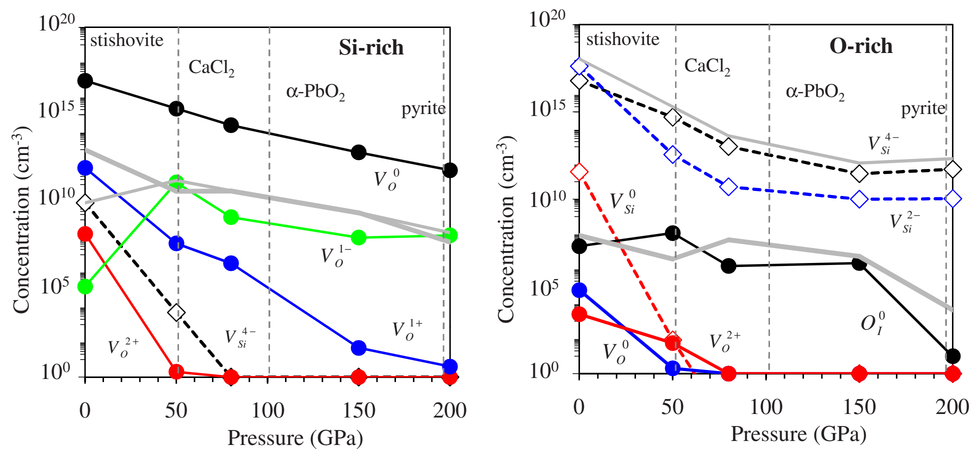

FIG. 2. (Color online) Estimated defect concentrations of the Si (open symbols) and O defects (solid symbols) as a function of pressure in the Si- (left) and O-rich (right) limits. The electron and hole concentrations are shown by thick and thin gray lines, respectively. The vertical lines at 52.2, 102.3, and 197.6 GPa represent the calculated phase boundaries.

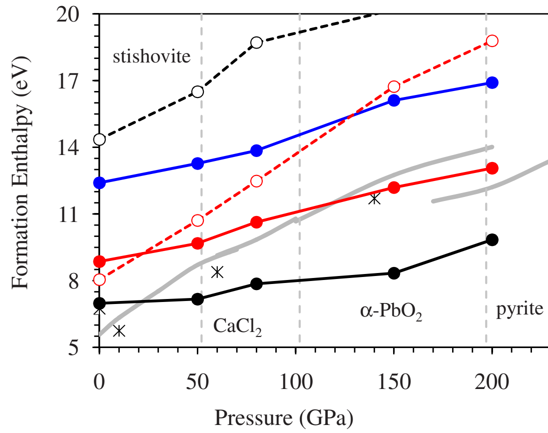

FIG. 3. (Color online) Formation enthalpies (per defect) of the Schottky triplet (gray line) and Frenkel pairs (lines with symbols) as a function of pressure. For O defects (solid lines), the bottom (black) line represents the neutral Frenkel defects. The middle (red) line represents the O^{2+}-Frenkel pair whereas the top (blue) line represents the O^{2-}-Frenkel pair. Similarly, for Si defects (dashed lines), the top (black) line represents the nuetral Frenkel pair whereas the lower (red) line represents the Si^{4+}-Frenkel pair. The SiO_2 pseudo-Schottky values derived for Mg_2SiO_4 at zero pressure (Ref. 15) and $MgSiO_3$ at high pressure (Ref. 17) are shown by asterisks. Note that Schottky defects were calculated at more pressures and up to 230 GPa.

Earth's mantle (2000–3000 K). At zero pressure for stishovite, the Fermi level is close to the mid band gap ($\mu_e = 2.89$ eV) in the Si-rich limit and it is thus jointly determined by the defects carrying positive and negative charges as well as holes and electrons. The major charged defects are $V_{\rm Si}^{4-}$, $V_{\rm O}^{2+}$, and $V_{\rm O}^{1+}$ but the concentration of neutral oxygen vacancies is the highest among all defects (Fig. 2, left). On the other hand, in the O-rich limit, the major defects are negatively charged Si vacancies and their concentrations along with the hole concentration determine the Fermi level, which is close to the VBM ($\mu_e = 0.88$ eV), (see Fig. 2, right). The concentrations of electrons and other defects including O defects and neutral defects are relatively low. The calculated position of the Fermi level changes with increasing pressure (Table I). In the $\lambda = 0$ limit, the Fermi level remains very close to the mid band gap. The neutral O defects continue to be dominant while the negatively charged O vacancies become more abundant as pressure increases. When $\lambda = 1$, the Fermi level moves away from VBM with increasing pressure but still remaining in the lower half of the band gap. Consistently, the concentrations of negatively charged defects (i.e., Si vacancies) and holes remain relatively high on compression.

Figure 3 shows the pressure variations of the calculated formation enthalpies of the Schottky triplets [Eqs. (9) and (10)] and different types of Frenkel pairs [Eqs. (11) and (12)] in different polymorphs. The formation enthalpies of all Frenkel defects increase with increasing pressure over the entire pressure regime studied. However, the Schottky defect formation enthalpy increases monotonically up to 150 GPa and then drops abruptly across the α-PbO_2 to pyrite phase transition by about 5 eV. Note that both $V_{\rm Si}^{4-}$ and $V_{\rm O}^{2+}$ formation enthalpies also drop across this transition. Since an overall trend is that the formation enthalpy in each case increases with increasing pressure, the corresponding activation volumes are positive. The values calculated by averaging over the entire pressure range studied are around 3.5, 4.5, and 2.0 cm^3/mol, respectively, for Schottky, Si-Frenkel and O-Frenkel defects. Among the charge-balanced stoichiometric complexes of defects, the Schottky triplet and the neutral O-Frenkel pair have the lowest enthalpies at 0 and 50 GPa, respectively, in stishovite. Neutral O-Frenkel defects are energetically most favorable in other high-pressure phases too. The formation enthalpies of these defect complexes are, in general, higher than the formation enthalpies of dominant individual defects (depending on the values of μ_e and λ). The concentrations of intrinsic defects of Schottky and Frenkel types, which are formed in a homogenous way in the close mode, are thus expected to be relatively low. Assuming an average formation enthalpy of 10 eV at pressures of the deep Earth's mantle, the estimated concentrations of the most favorable defects at 3000 K are in the order of 10^5 defects per cm^3. Although direct contributions to the electrical conductivity from ionic vacancies are too small, these defects can serve as favorable sites for proton incorporation[30] and can control the creep process.[12,13]

B. Migration enthalpies

The ion migration enthalpy was calculated using the nudged-elastic-band method,[31] which works by considering a series of configurations (images) corresponding to a trajectory of an ion migrating between two potential minima (corresponding two vacancy or interstitial sites). To find the minimum-energy migration path, all configurations were concurrently optimized to minimize their total energies by constraining the ionic relaxations so as to reduce the total force components that act in the directions perpendicular to the hypertangent between the two neighboring configurations until these force components become zero. We calculate the migration enthalpies for Si and O ions for both the vacancy-to-vacancy and interstitial-to-interstitial mechanisms (Fig. 4). The vacancy and interstitial migration enthalpies at 0 GPa are 4.45 and 0.92 eV, respectively, for Si^{4+} ions. The neutral Si vacancy and interstitial migrations have similar values (4.36 and 0.95 eV, respectively). The vacancy and interstitial migration enthalpies are 0.81 and 0.34 eV, respectively, for O^{2-} ions. Unlike the Si ions, the migration enthalpies for neutral O vacancy and interstitial defects are much larger (5.22 and 0.61 eV) than those for the charge state. Similar comparisons hold at 200 GPa. Therefore, we calculate the migration enthalpies of Si and O ions only in their charged states as a function of pressure (Fig. 4). The calculated values correspond to the activation enthalpies in the extrinsic diffusion regime in which defects are assumed to already be present in the system. All migration enthalpies show the general trend of increasing with pressure so the average activation volumes of Si and O diffusion are mostly positive expect at very high pressures. In particular, the Si vacancy migration enthalpy decreases at the $CaCl_2$ to α-PbO_2 phase transition whereas other migration enthalpies drop abruptly at the

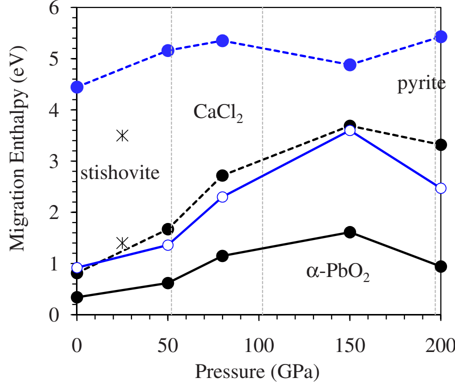

FIG. 4. (Color online) Activation enthalpies of Si^{4+} (open symbols) and O^{2-} (closed symbols) ions for the vacancy-to-vacancy (dashed lines) and interstitial-to-interstitial (solid lines) migrations. The experimental data measured in silicates at about 22 GPa are shown for silicon (Ref. 33) and oxygen (Ref. 34) by upper and lower asterisks, respectively.

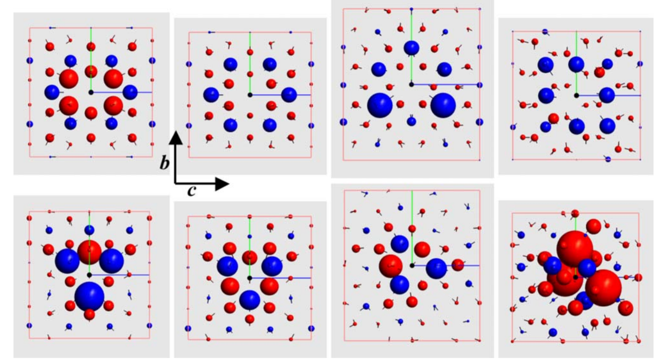

FIG. 5. (Color online) Lattice distortions due to V_{Si}^{4-} (upper row) and V_{O}^{2+} (lower row) defects for stishovite at 0 GPa, $CaCl_2$ phase at 80 GPa, α-PbO_2 phase at 150 GPa, and pyrite phase at 200 GPa (from left to right). Blue and red spheres denote Si and O atoms, respectively, whereas the black sphere at the center denotes the defect site. The sphere size and line orientation encode atomic displacements.

α-PbO_2 to pyrite phase transition. Our results are comparable with previous calculations[17,32] and experimental[33,34] data for silicates at high pressure.

In a perfect crystal the defects can be created by two ways. First, in a closed system, intrinsic defects are formed in a homogenous way in the form of Schottky triplet and Frenkel pairs. Second, in an open system, defects are formed in a heterogeneous way through reactions with the external environments. Diffusion may involve either the vacancy or the interstitial or both mechanisms. The activation enthalpy for self-diffusion of ion of type X (in the charge state q) is determined by the sum of the formation and migration enthalpies of the corresponding defect. In the closed mode, the diffusion activation enthalpy for vacancy mechanism involving the Schottky triplets is given by

$$H_d^V(X^q,P) = H_f^S(P) + H_m^V(X^q,P), \tag{14}$$

where X is Si ion (q=4+) or O ion (q=2−). For the Frenkel pairs, the activation enthalpies for vacancy and interstitial mechanisms are, respectively, given by

$$H_d^V(X^q,P) = H_f^F(X^q,P) + H_m^V(X^q,P), \tag{15}$$

$$H_d^I(X^q,P) = H_f^F(X^q,P) + H_m^I(X^q,P). \tag{16}$$

The activation enthalpies for Si diffusion at 0 GPa are 10.03 eV for vacancy migration from Schottky triplets, and 12.50 and 8.97 eV, respectively, for vacancy and interstitial migration from Frenkel pairs. Similarly, the activation enthalpies for O diffusion are 6.39 eV for vacancy migration from Schottky triplets, and 9.67 and 9.20 eV, respectively, for vacancy and interstitial migration from Frenkel pairs. But in the open mode, the dominant mechanism depends on the external environment. In the Si-rich condition, the activation enthalpies for Si diffusion are 9.5 and 11.9 eV, respectively, for vacancy and interstitial migration, and the corresponding numbers are 5.8 and 11.85 eV for O diffusion. On the other hand, in the O-rich condition the activation enthalpies for Si diffusion are 5.5 and 15 eV, respectively, for vacancy and interstitial migration, and the corresponding numbers are 8.6 and 10.8 eV for O diffusion.

C. Structural distortions

To analyze lattice distortions around defects, atomic displacement data of defective systems relative to the corresponding perfect systems are visualized (see Fig. 5). Atoms are shown as spheres whose size is proportional to the magnitude of displacement and the orientation of lines originating from sphere surface indicates the direction of displacement. Different phases show different patterns and degrees of distortion. At zero pressure, the maximum displacements due to Si and O vacancies are, respectively, 8% and 13% for stishovite, and in high-pressure phases, most of the defect-induced distortion is accommodated by the movement of the nearest- and the next-nearest-neighbor atoms. In stishovite, four out of six octahedral O atoms around Si vacancy site are pushed away significantly and also the Si atoms that share the octahedral edge with vacancy site see large displacements. The distortion due to the O vacancy consists of large displacements of three nearest-neighbor Si atoms as well as their octahedral O atoms. Very similar structures (but with much smaller atomic displacements) are shown by vacancies in $CaCl_2$ phase. Defect-induced atomic structures in α-PbO_2 and pyrite phases are quite different from those of stishovite. For instance, the next-nearest Si neighbors of the Si vacancy site move much more than the nearest O neighbors in both phases. In pyrite-type phase, the next-nearest O neighbors of the O vacancy site move more than the nearest Si neighbors; 16% of equilibrium bond lengths at 200 GPa. Atomic structure of a migrating ion represents to a great extent superposition of displacement patterns of two vacancy sites with the ion placed at the saddle point between two sites. For example, in stishovite two O atoms nearest to the migrating Si ion are pushed away in a direction perpendicular to the migration direction by the largest amounts, and so are two Si atoms nearest to the migrating O atom (Fig. 6). In both cases, the displacement patterns on either side of the migrating ion

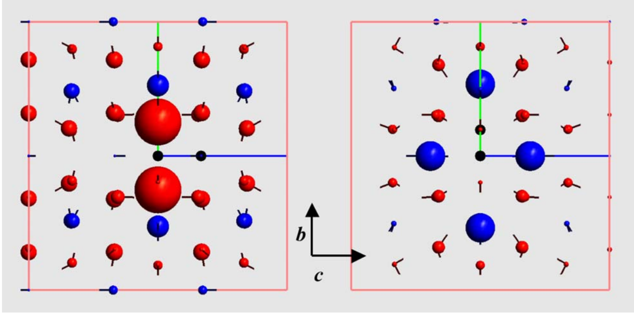

FIG. 6. (Color online) Lattice distortions due to the migrating Si (left) and O (right) ions for stishovite at 0 GPa. Blue and red spheres denote Si and O atoms, respectively. The black sphere at the center denotes the migrating ion and other black sphere represents one of the vacancy sites whereas the vacancy site on the other side of the ion is not shown.

positions resemble to a great extent the part (roughly one half) of the structure of the corresponding vacancy defect.

D. Electronic structures

We study the electronic structures of defects by calculating the projected density of states (PDOS) and squared eigenwave functions. First, for a perfect supercell of stishovite at zero pressure, the lower and upper valence bands in PDOS (Fig. 7, top) primarily represent the O 2*s* and O 2*p* states, respectively, with minor contributions from Si states. The contributions of Si 3*s*, 3*p* and 3*d* states are important, respectively, at low-, mid- and high-energy regions of each

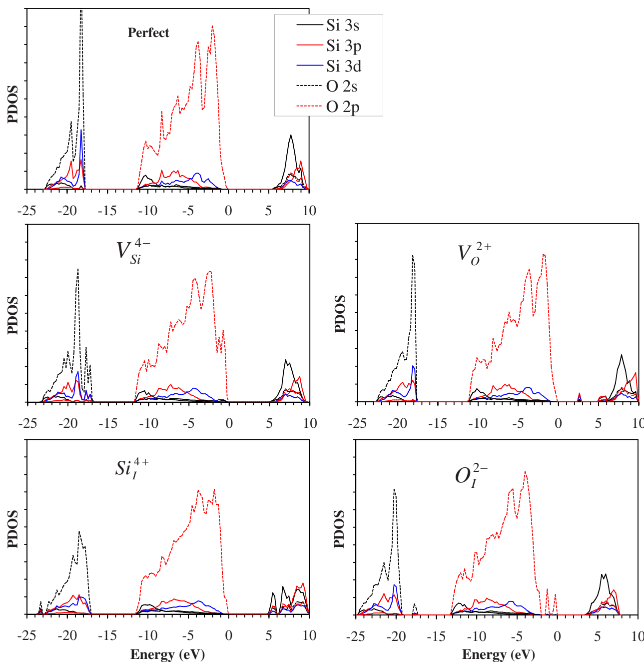

FIG. 7. (Color online) Projected density of states of the perfect and defective supercells of stishovite at 0 GPa. The 3*s*, 3*p*, and 3*d* contributions from Si atoms and the 2*s* and 2*p* contributions from O atoms are shown. The top of the valence band of each case is set zero.

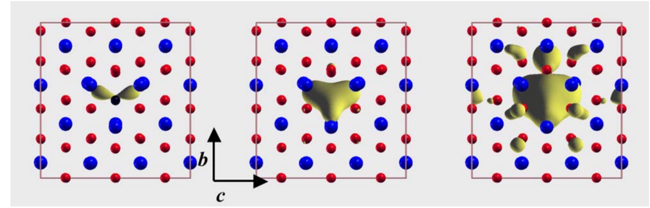

FIG. 8. (Color online) Squared eigenfunction of the defect level at the gamma point of Brillouin zone for V_O^{2+}. The isosurfaces from the left to the right are for high, mid, and small values of the squared eigenfunctions. The blue (large) and red (small) spheres denote Si and O atoms, respectively. The black sphere is the defect site.

band. The predicted band gap of 5.76 eV is likely to be underestimated significantly as generally expected. A very similar value of 5.70 eV was previously calculated.[36] The conduction band toward its bottom comprises of hybridized states with major contribution from the Si 3*s* state.

The PDOS shapes of the defective supercell containing V_{Si}^{4-} differ considerably from those of the perfect crystal (Fig. 7, middle left). Both the valence bands tend to extend to higher energy due to vacancy-induced distortion in potentials seen by the neighboring atoms. For instance, the O 2*s* component in the upper valence band shows two shoulder peaks on high-energy side. The states spilling out from the VBM represent acceptorlike shallow defect states. In the case of V_O^{2+}, the PDOS shapes of the valence bands are very similar to those of perfect crystal but a defect band appears near the mid band gap (Fig. 7, middle right). Note that the defect band would correspond to a defect state in an infinite crystal containing a single vacancy. It represents hybridization of Si 3*p* and 3*d*, and O 2*p* orbitals. The state is above the Fermi level (i.e., above the VBM) but it can serve as acceptorlike shallow defect state. The integration of total DOS in this energy region suggests that the defect state can accommodate a pair of electrons. The localized character of the electrons, which would be trapped in the vacancy, is confirmed by plotting the squared eigenfunction of the defect level at gamma point (Fig. 8). The squared eigenfunction shows two regions of relatively large values near the vacancy site representing most of the electron localization. Its values though small in the regions away from the vacancy suggest that the corresponding electron density tends to delocalize toward three nearest Si atoms. However, the electronic structure does not show a threefold symmetry, consistent with the atomic structure of the defect (Fig. 5). Note that these Si atoms share the vacancy site as the polyhedral corner-sharing O atom. We also study the electronic structure of the neutral oxygen vacancy. A defect state appears in the band gap and the state is filled up with two electrons showing a strong localized character. Thus, V_O^{2+} means the removal of an O atom along with two electrons, which would otherwise occupy the mid gap defect state and be localized in the vacancy site. The states spill out from the CBM forming a bump and they comprise of primarily Si 3*s* and 3*p* states. The PDOS shapes are strongly affected by the Si and O interstitials. For I_{Si}^{4+}, the valence bands get widen and the conduction band extends into the band gap with the appearance of well-defined peak

at the CBM with dominance of 3*s* states (Fig. 7, bottom left). On the other hand, the I_O^{2-} defect introduces the states just above the top of both the lower and upper valence bands (Fig. 7, bottom right). The integration of the total DOS in the corresponding energy regions gives two and four electrons filling up these deep and shallow defect states, respectively. Moreover, as in V_O^{2+}, these electrons show strong localized character.

The effects of pressure on the calculated PDOS are systematic. The valence bands get widen and the gap between them decreases with compression. However, the gap between the valence and conduction bands increasingly opens with compression. The PDOS shapes of all bands and relative contributions from different states remain essentially unaffected. For instance, the defect-induced state (band) for O defects appear in the band gap or above the valence band at all pressures (and in other polymorphs) with its position somewhat shifted in one way or other.

IV. CONCLUSIONS

We have presented important results and discussion on energetics, geometric, and electronic structures of a wide variety of native point defects in the form of vacancies, interstitials and their stoichiometric complexes in silica within density-functional theory. Four polymorphs of silica, namely, stishovite, $CaCl_2$, α-PbO_2, and pyrite types were simulated in the pressure range of 0 to 200 GPa. The formation enthalpies of the isolated defects were shown to differ substantially between the Si- and O-rich limits, for instance, the differences are as large as 10.8 and 5.4 eV, respectively, for Si and O defects at zero pressure. For charged states, the enthalpies also depend on the Fermi level, whose position itself is determined by the charge neutrality between concentrations of electrons, holes and charged defects at a given temperature. The defect complexes, in particular, the Schottky triplets and various types of Frenkel pairs were studied. Unlike the individual vacancies and interstitials, these complexes being independent of atomic chemical potentials and electron potential have well-defined energies. Our results show that the formation enthalpies increase by a factor of 2 over the entire pressure range. Most enthalpies increase across the phase transitions but some vacancy and Schottky defect formation enthalpies decrease across the α-PbO_2 to pyrite phase transition. The Schottky triplets are energetically most favorable at zero pressure but O-Frenkel pairs become systematically more favorable at higher pressures. The average activation volume of Schottky defects lies between the activation volumes of Si-Frenkel and O-Frenkel pairs. The nudged-elastic-band method—a more efficient approach compared to the simple midpoint method was used to calculate the migration enthalpies. The results suggest that the interstitial mechanisms are favored over the vacancy hoping mechanisms. The defects and migrating ions were shown to induce substantial structural distortions, which are absorbed mostly by the nearest- and next-nearest-neighbor atoms. The atomic displacement patterns show large differences between different phases. Examination of projected density of states and the squared eigenfunctions suggests that the electronic structures vary largely among different defect types. In particular, O defects induce defect state in the band gap, which causes charge localization around the defect center. The electronic structures remain qualitatively unchanged with compression showing similar trends among different polymorphs.

ACKNOWLEDGMENTS

This work was supported by the NSF Career grant (Grant No. EAR 0347204). Computing facility was provided by CCT at Louisiana State University.

*Permanent address: High Pressure Physics Division, Bhabha Atomic Research Centre, Mumbai 400085, India.

[1] A. R. Oganov, M. J. Gillan, and G. D. Price, Phys. Rev. B **71**, 064104 (2005).
[2] B. B. Karki, M. C. Warren, L. Stixrude, G. J. Ackland, and J. Crain, Phys. Rev. B **55**, 3465 (1997); **56**, 2884(E) (1997).
[3] Y. Kuwayama, K. Hirose, N. Sata, and Y. Ohishi, Science **309**, 923 (2005).
[4] R. A. Weeks and C. M. Nelson, J. Am. Ceram. Soc. **43**, 399 (1960).
[5] J. K. Rudra, W. B. Fowler, and F. Feigl, Phys. Rev. Lett. **55**, 2614 (1985).
[6] A. M. Stoneham, M. A. Szymanski, and A. L. Shluger, Phys. Rev. B **63**, 241304 (2001).
[7] C. M. Carbonaro, V. Fiorentini, and F. Bernardini, Phys. Rev. Lett. **86**, 3064 (2001).
[8] Y.-G. Jin and K. J. Chang, Phys. Rev. Lett. **86**, 1793 (2001).
[9] G. Roma and Y. Limoge, Phys. Rev. B **70**, 174101 (2004).
[10] D. R. Hamann, Phys. Rev. Lett. **81**, 3447 (1998).
[11] S. Karato, M. S. Paterson, and J. D. FitzGerald, J. Geophys. Res. **91**, 8151 (1986).
[12] F. Bejina, O. Jaoul, and R. C. Liebermann, J. Geophys. Res. **104**, 25529 (1999).
[13] R. S. Gordon, *In Point Defects in Minerals*, Geophysical Monograph Series, edited by R. N. Schock (AGU, Washington, D.C., 1985) Vol. 31, p. 132.
[14] D. P. Dobson and J. P. Brodholt, J. Geophys. Res. **105**, 531 (2000); S. Constable and A. Duba, Phys. Chem. Miner. **29**, 446 (2002).
[15] J. P. Brodholt, Am. Mineral. **82**, 1049 (1997).
[16] S. Ogut and J. R. Chelikowsky, Phys. Rev. B **64**, 245206 (2001).
[17] B. B. Karki and G. Khanduja, Modell. Simul. Mater. Sci. Eng. **14**, 1041 (2006); Earth Planet. Sci. Lett. **260**, 201 (2007).
[18] A. De Vita, M. J. Gillan, J. S. Lin, M. C. Payne, I. Stich, and L. J. Clarke, Phys. Rev. B **46**, 12964 (1992).
[19] http://www.pwscf.org.
[20] H. J. Monkhorst and J. D. Pack, Phys. Rev. B **13**, 5188 (1976).
[21] D. M. Ceperley and B. J. Alder, Phys. Rev. Lett. **45**, 566 (1980); J. P. Perdew and Y. Wang, Phys. Rev. B **45**, 13244 (1992).
[22] S. Mukherjee, R. R. Cohen, and O. Gulseren, J. Phys.: Condens.

Matter **15**, 855 (2003).
[23] D. Alfe and M. J. Gillan, Phys. Rev. B **71**, 220101 (2005).
[24] R. M. Nieminen, in *Theory of Defects in Semionductors*, (Springer, Berlin/Heidelberg, 2007) Vol. 104, p. 29.
[25] S. B. Zhang and J. E. Northrup, Phys. Rev. Lett. **67**, 2339 (1991).
[26] A. Togo, F. Oba, I. Tanaka, and K. Tatsumi, Phys. Rev. B **74**, 195128 (2006).
[27] M. Leslie and M. J. Gillan, J. Phys. C **18**, 973 (1985).
[28] J. Lento, J. L. Mozoz, and R. M. Nieminen, J. Phys.: Condens. Matter **14**, 2637 (2002).
[29] C. Lee and X. Gonze, Phys. Rev. B **56**, 7321 (1997).
[30] X. Huang, Y. Xu, and S. Karato, Nature (London) **434**, 746 (2005).
[31] H. Johsson, G. Mills, and K. M. Jacobsen, in *Nudged Elastic Band Method for Finding Minimum Energy Paths of Transitions in Classical and Quantum Dynamics in Condensed Phase Simulations*, edited by B. J. Berne, G. Ciccotti, and D. F. Coker (World Scientific, Singapore, 1998).
[32] G. W. Watson, A. Wall, and S. C. Parker, J. Phys.: Condens. Matter **12**, 8427 (2000); K. Wright and G. D. Price, J. Geophys. Res. **98**, 22245 (1993).
[33] D. Yamazaki, T. Kato, H. Yurimoto, E. Ohtani, and M. Toriumi, Phys. Earth Planet. Inter. **119**, 299 (2000).
[34] D. Dobson, Phys. Earth Planet. Inter. **139**, 55 (2003).
[35] M. A. Spackman, R. J. Hill, and G. V. Gibbs, Phys. Chem. Miner. **14**, 139 (1987).
[36] R. E. Cohen, Am. Mineral. **76**, 733 (1991).